Received: 2 August 2023 | Revised: 21 December 2023 | Accepted: 26 January 2024

DOI: 10.1002/mp.17010

RESEARCH ARTICLE

MEDICAL PHYSICS

Optimizing dual-energy CT technique for iodine-based contrast-to-noise ratio, a theoretical study

Fatma Terzioglu[1] | **Emil Y. Sidky**[2] | **John Paul Phillips**[2] | **Ingrid S. Reiser**[2] | **Guillaume Bal**[3] | **Xiaochuan Pan**[2]

[1]Department of Mathematics, North Carolina State University, Raleigh, North Carolina, USA

[2]Department of Radiology, The University of Chicago, Chicago, Illinois, USA

[3]Departments of Statistics and Mathematics, The University of Chicago, Chicago, Illinois, USA

Correspondence
Fatma Terzioglu, Department of Mathematics, North Carolina State University, 2311 Stinson Dr., Raleigh, NC 27695, USA.
Email: fterzioglu@ncsu.edu

Funding information
National Science Foundation, Grant/Award Numbers: DMS-2206279, DMS-2306411, DMS-1908736; National Institutes of Health, Grant/Award Numbers: R01-EB023968, R21-CA263660

Abstract

Background: Dual-energy CT (DECT) systems provide valuable material-specific information by simultaneously acquiring two spectral measurements, resulting in superior image quality and contrast-to-noise ratio (CNR) while reducing radiation exposure and contrast agent usage. The selection of DECT scan parameters, including x-ray tube settings and fluence, is critical for the stability of the reconstruction process and hence the overall image quality.

Purpose: The goal of this study is to propose a systematic theoretical method for determining the optimal DECT parameters for minimal noise and maximum CNR in virtual monochromatic images (VMIs) for fixed subject size and total radiation dose.

Methods: The noise propagation in the process of projection based material estimation from DECT measurements is analyzed. The main components of the study are the mean pixel variances for the sinogram and monochromatic image and the CNR, which were shown to depend on the Jacobian matrix of the sinograms-to-DECT measurements map.

Analytic estimates for the mean sinogram and monochromatic image pixel variances and the CNR as functions of tube potentials, fluence, and VMI energy are derived, and then used in a virtual phantom experiment as an objective function for optimizing the tube settings and VMI energy to minimize the image noise and maximize the CNR.

Results: It was shown that DECT measurements corresponding to kV settings that maximize the square of Jacobian determinant values over a domain of interest lead to improved stability of basis material reconstructions.

Instances of non-uniqueness in DECT were addressed, focusing on scenarios where the Jacobian determinant becomes zero within the domain of interest despite significant spectral separation. The presence of non-uniqueness can lead to singular solutions during the inversion of sinograms-to-DECT measurements, underscoring the importance of considering uniqueness properties in parameter selection.

Additionally, the optimal VMI energy and tube potentials for maximal CNR was determined. When the x-ray beam filter material was fixed at 2 mm of aluminum and the photon fluence for low and high kV scans were considered equal, the tube potential pair of 60/120 kV led to the maximal iodine CNR in the VMI at 53 keV.

Conclusions: Optimizing DECT scan parameters to maximize the CNR can be done in a systematic way. Also, choosing the parameters that maximize the Jacobian determinant over the set of expected line integrals leads to more stable reconstructions due to the reduced amplification of the measurement noise. Since the values of the Jacobian determinant depend strongly on the imaging task, careful consideration of all of the relevant factors is needed when implementing the proposed framework.

KEYWORDS
dual-energy CT, iodine based contrast-to-noise ratio, optimal parameter design

1 | INTRODUCTION

Dual-energy CT (DECT) systems enable the simultaneous acquisition of two spectral measurements to identify different materials within the scanned object. DECT has been demonstrated to outperform single-energy CT in terms of image quality and contrast-to-noise ratio (CNR), allowing for reduced radiation exposure and contrast agent concentration while maintaining image quality.[1–5] The concept of DECT was introduced by Hounsfield in the 1970s,[6] and the mathematical framework for pre-reconstruction processing of DECT data was developed by Alvarez and Macovski in a seminal paper in 1976.[7] Their approach to material decomposition is based on the assumption that energy-dependent attenuation coefficients of chemical compounds can be approximated by a linear combination of elemental mass attenuation maps weighted by the partial density of each element.

In this paper, we focus on projection-based material decomposition in DECT, which involves the estimation of line integral values by solving a nonlinear system of equations for each x-ray path before applying filtered-back projection (FBP) algorithm to reconstruct each material density map. The second step, applying FBP, is a linear inverse problem whose uniqueness properties are well-studied. However, due to the nonlinearity of the mapping from line integrals to DECT measurements, referred to as the sinogram-to-DECT mapping hereinafter, the uniqueness of the estimated line integral values is not guaranteed. An example of non-unique solutions in DECT was first provided by Levine[8] for a material basis of water and bone using spectra with three discrete photon energies. Later, Alvarez[9] analyzed the invertibility of the sinogram-to-DECT mapping by testing nonvanishing of its Jacobian determinant values within the domain of interest. In general, the nonvanishing of the Jacobian determinant guarantees only local uniqueness (a.k.a. injectivity), requiring additional constraints for global uniqueness. Bal and Terzioglu[10] presented sufficient analytic criteria for the global injectivity of multi-energy CT (MECT) measurement map for a given number of materials and equal number of energy measurements. In the case of DECT, they proved that the nonvanishing of the Jacobian determinant of the sinogram-to-DECT mapping throughout its domain is sufficient to ensure global uniqueness. They also demonstrated how the choice of basis materials and x-ray spectra influences the Jacobian determinant values and, consequently, the invertibility. In this paper, we showcase the occurrence of non-uniqueness despite significant separation in x-ray spectra. The provided example illustrates that it is possible to have two isolated line integral values corresponding to the same DECT measurement pair when the Jacobian determinant vanishes inside a rectangular region encompassing all expected line integral values.

It was shown by Bal et al.[11] that the inversion stability of the sinogram-to-DECT mapping is improved by choosing the x-ray spectra that maximize Jacobian determinant values of this transformation over a domain of interest. In this paper, we propose a systematic method for determining optimal tube settings and fluence that minimize noise and maximize CNR in material density images obtained from DECT scans while keeping subject size and total radiation dose fixed. To achieve this, we consider a noise model based on a compound Poisson process for the DECT measurements and analyze the noise propagation from DECT measurements to material density images by linearizing the inverse sinogram-to-DECT mapping. We derive analytic expressions for sinogram and monochromatic image pixel variances as functions of tube potentials, fluence, and virtual monochromatic image (VMI) energy. These expressions, along with CNR, are used to optimize the tube settings and VMI energy. Through a virtual phantom experiment for iodine-water material pair, we found the optimal VMI energy corresponding to the least noisy monochromatic image synthesized from iodine and water density images.

The problem of improving iodine CNR in VMI has been previously addressed. The works by Leng et al.[2] and Tao et al.[12] focused on applying denoising techniques during the reconstruction process. Yu et al.[13,14] examined the effect of subject size and photon fluence on the image quality of linearly mixed images generated from DECT scans using a dual-source CT scanner, assuming a fixed x-ray source kilovoltage-peak (kV)

setting and total radiation dose. Michalak et al.[15] conducted a phantom study to empirically determine the optimal photon energies for virtual mono-energetic imaging across various phantom sizes. Dabli et al.[16] empirically determined optimal tube settings that yield high image quality and accuracy for low iodine concentration quantification. Ren et al.[17] analyzed the conditioning of spectral weights by employing singular value decomposition of the matrix formed by sampling the intensity profile of each spectral weight over the energy range. Our approach differs from the above studies in terms of the analysis methods employed. Specifically, we analyze noise propagation, derive variance expressions, and use them to optimize tube settings, ultimately identifying the optimal VMI energy for maximal CNR and least noisy monochromatic images.

2 | METHODS

In this section, we detail the approaches and procedures employed to optimize DECT scan parameters for improved iodine-based CNR. We first present the physical model for the DECT measurements, considering the well-established assumption of the basis material decomposition[7,18] and a noise model based on the compound Poisson process.[19] Next, we explore the role of the Jacobian matrix in ensuring reconstruction uniqueness and examine noise propagation by linearizing the inverse sinogram-to-DECT mapping. We then derive analytical expressions for CNR, mean sinogram variance, and mean pixel variance. We finally show that the smallest eigenvalue of the mean pixel covariance matrix gives the minimum mean variance for the monochromatic image, which enables us to simplify the task of determining the optimal tube settings. We conclude the section by outlining the setup for our numerical simulations.

2.1 | Scan configuration, DECT technique, and noise simulation

The physics modeling for the DECT system includes available models for Tungsten x-ray source spectra, low and high kV fluence, response of energy-integrating detectors, and compound Poisson noise.[19]

For iodine-based contrast imaging with a DECT system, we assume that the scanned object is composed of iodine and water only. Consequently, the linear attenuation coefficient is approximated by[7]

$$\mu(E, y) \approx M_1(E)\rho_1(y) + M_2(E)\rho_2(y), \tag{1}$$

where $M_1(E)$ and $M_2(E)$ denote material attenuation at energy E for iodine and water, respectively, and $\rho_1(y)$ and $\rho_2(y)$ are their mass density at a spatial location y. While the mass densities are unknown and need to be reconstructed, the energy dependent attenuation maps are known a priori, which are available at the NIST database.[20] To simplify the notation, we write

$$M(E) = \begin{bmatrix} M_1(E) \\ M_2(E) \end{bmatrix}.$$

For a given x-ray beam l, the line integral of mass density ρ_j of the j-th material is given by $x_j(l) = \int_l \rho_j(y)dy$. We let

$$x = x_l = \begin{bmatrix} x_1(l) \\ x_2(l) \end{bmatrix}.$$

Let $S_1(E)$ and $S_2(E)$ be the x-ray energy spectra corresponding to low and high energy x-ray tube potentials tp_1 and tp_2, respectively. The x-ray spectra used in the experiments were known a priori, which were modeled, for given tube potentials, by using the publicly available Python software toolkit SpekPy v2.0.[21]

For an x-ray beam I, the number of photons incident on the detector with energy E per unit time corresponding to the i-th measurement is given by

$$I_i(x_l; E) = S_i(E)e^{-\int_l \mu(E,y)dy} \approx S_i(E)e^{-M(E)\cdot x_l}, \quad i = 1, 2, \tag{2}$$

where $M(E) \cdot x_l = M_1(E)x_1(l) + M_2(E)x_2(l)$.

The total number of detected photons associated to line l is then given by

$$I_i(x_l) = \int_0^\infty S_i(E)e^{-M(E)\cdot x_l} D(E)dE, \quad i = 1, 2, , \tag{3}$$

where $D(E)$ is the energy dependence of the detector sensitivity. For energy integrating detectors, $D(E) = \alpha E$ for some positive constant α.[19]

In this study, we consider the negative logarithm of the intensity measurements, which we refer to as the sinogram-to-DECT mapping,

$$g_i(x) = -\ln I_i(x), \quad i = 1, 2. \tag{4}$$

We define

$$I(x) = \begin{bmatrix} I_1(x) \\ I_2(x) \end{bmatrix}, \qquad g(x) = \begin{bmatrix} g_1(x) \\ g_2(x) \end{bmatrix}.$$

We consider the line integral values $x = x_l \in \mathcal{R} = [0, a_1] \times [0, a_2]$, where $\mathcal{R}$ a is rectangle in $\mathbb{R}^2$, and a_j represents the maximum noise-free line integral value expected for the j-th material for a particular imaging task. Therefore, the rectangle $\mathcal{R}$ needs to be large enough to encompass all possible material thicknesses for a given category of scanned objects, such as the breast in dedicated breast CT or wrist, knee, or elbow in extremity imaging.

In the reconstruction of mass density maps from DECT measurements, we consider a two step material decomposition method illustrated in the following diagram:

$$\begin{bmatrix} g_1 \\ g_2 \end{bmatrix} \xrightarrow[\text{method}]{\text{Newton's}} \begin{bmatrix} x_1 \\ x_2 \end{bmatrix} \xrightarrow[\text{back-projection}]{\text{Filtered}} \begin{bmatrix} \rho_1 \\ \rho_2 \end{bmatrix}. \quad (5)$$

That is, for each line l, we first apply Newton's method to recover the line integral values, and then use FBP algorithm to reconstruct the material density maps.

For $i = 1, 2$, the spectral measurements I_i are assumed to be independent random variables that follow a compound Poisson process.[19] The covariance matrix for the log-intensity measurements g is then given by

$$\Sigma_g(x) = \begin{bmatrix} \sigma_g(x)_1^2 & 0 \\ 0 & \sigma_g(x)_2^2 \end{bmatrix}, \quad (6)$$

where

$$\sigma_g(x)_i^2 = \frac{\int_0^\infty D^2(E)S_i(E)e^{-M(E)\cdot x}dE}{\left(\int_0^\infty D(E)S_i(E)e^{-M(E)\cdot x}dE\right)^2}, \quad (7)$$

is the variance of the i-th log-intensity measurement g_i, $i = 1, 2$.

We note that Σ_g depends on the detector sensitivity $D(E)$ but is independent of the factor α.

2.2 | Jacobian of the sinogram-to-DECT mapping and uniqueness of inversion

Due to the nonlinearity of Equation (3) with respect to line integral values x_l, DECT measurements may not always result in a unique model inverse. This lack of uniqueness can lead to different line integral values producing the same transmission measurement value, potentially leading to incorrect material density map reconstructions. To prevent this, one can select scan parameters that ensure measurements always lead to unique inversion of the transmission model. In fact, for nonlinear maps defined on convex domains, local constraints on the Jacobian of the forward measurements provide sufficient criteria for uniqueness.[22–24]

In our case, the map $x \to g(x)$ is smooth and its Jacobian matrix at point $x \in \mathcal{R}$ is given by the matrix $J(x)$ with entries

$$J_{ij}(x) = \frac{\partial g_i}{\partial x_j}(x) = \frac{\int_0^\infty D(E)S_i(E)M_j(E)e^{-M(E)\cdot x}dE}{\int_0^\infty D(E)S_i(E)e^{-M(E)\cdot x}dE}, \quad i, j = 1, 2. \quad (8)$$

Based on the work of Gale and Nikaido,[22] Bal and Terzioglu[10] proved that if the Jacobian determinant

$$\det J(x) = J_{11}(x)J_{22}(x) - J_{12}(x)J_{21}(x) \neq 0, \quad (9)$$

for all $x \in \mathcal{R}$, the map $x \to g(x)$ is globally injective. This means that the estimation of x from the knowledge of $g(x)$ (or $I(x)$) is unique.

In DECT, the values of the Jacobian determinant depend on the material basis and the x-ray spectra.[10] For iodine-water material pair, we demonstrate the dependence of the Jacobian determinant on the x-ray spectra in Figures 1 and 2 of Section 3.1. We also present in Figure 3 an example scan protocol where the uniqueness does not hold. That is, the Jacobian determinant vanishes inside the rectangle and there exist two distinct line integral values that are mapped by g to the same measurement pair.

2.3 | Noise propagation based on linearization of the inverse sinogram-to-DECT mapping

In the following, we present an analysis of the noise propagation from DECT measurements to the estimated sinograms by considering first order Taylor approximation to inverse sinogram-to-DECT mapping.

For a given line integral value $x_l \in \mathcal{R}$ corresponding to a line l, and a noise vector η, we let $g^\eta(x_l)$ denote the noisy DECT measurement:

$$g^\eta(x_l) = g(x_l) + \eta. \quad (10)$$

Let x_l^η be the line integral value that is estimated from $g^\eta(x_l)$. Assuming that the noise is small and considering a first order Taylor expansion, we have

$$x_l^\eta \approx x_l + J^{-1}(x_l)\eta. \quad (11)$$

Under the linearization regime, the 2×2 covariance matrix of the estimated line integral values is given by

$$\Sigma_l = \Sigma_{x_l} = J^{-1}(x_l)\Sigma_{g^\eta}(x_l)J^{-t}(x_l), \quad (12)$$

where $-t$ denotes the transpose of inverse matrix (see e.g., Cowan, p. 21).[25] Here, the diagonal entries of (12) are the variances of the iodine and water sinograms, and the off-diagonal entries are the covariance between them (see, e.g., Roessl et al.[26] for their explicit formulas).

We define the diagonal matrices iodine and water sinogram variances and covariance as $C^{(ij)}$, $i, j = 1, 2$. Therefore,

$$(C^{(ij)})_{ll} = (\Sigma_l)_{ij}, \quad i, j = 1, 2. \quad (13)$$

We also define a matrix $Q = (q_{ij})_{i,j=1,2}$ with diagonal entries being the mean pixel variance of each material density map whereas the off-diagonal entries are the mean covariance between them. Let $B = (b_{pl})_{1\le p\le P,\ 1\le l\le L}$ denote the FBP matrix. Then,

$$q_{ij} = \frac{1}{P}\mathrm{tr}(BC^{(ij)}B^t), \quad j = 1, 2. \tag{14}$$

It is well known that the acquisition of photons for each spectral measurement may be shortened or lengthened to minimize estimation errors. Let T be the total time of acquisition and let τ be the acquisition time of the low energy measurement, where $0 < \tau < T$, (so that $T - \tau$ is the time of acquisition in the high kV setting). Since the variance of the measurement noise is proportional to photon count, we observe that the covariance matrix of the measurement error is divided by τ when $i = 1$ and $T - \tau$ with $i = 2$. We thus have a modified covariance matrix for the estimated sinograms

$$\Sigma_l = J^{-1}(x_l)F\Sigma_{g^\eta}(x_l)J^{-t}(x_l), \tag{15}$$

where

$$F = \begin{bmatrix} \tau & 0 \\ 0 & T-\tau \end{bmatrix}.$$

It is important to note that the matrix Σ_l is always symmetric, and is also positive definite provided that $\det J(x_l) \neq 0$. We also observe from Equations (12) and (15) that the sinogram (co-)variances are inversely proportional to the square of the Jacobian determinant. Therefore, optimizing DECT scan parameters to maximize the minimum value of the Jacobian determinant over the sinogram domain leads to more stable sinogram estimation due to the reduced amplification of the measurement noise (also see, Bal et al.[11]).

2.4 | Computation of pixel variances and the CNR of a monochromatic image

Once the sinograms x_1 and x_2 (for iodine and water, respectively) are reconstructed from the DECT measurements using a nonlinear iterative algorithm, for which we use Newton's method in this study, they can be combined linearly to obtain a monochromatic sinogram, that is

$$x_{mono} = w_1x_1 + w_2x_2 = w^tx, \tag{16}$$

where $w = [w_1, w_2]^t$ is a unit vector in $\mathbb{R}^2$, that is, $\|w\|_2 = 1$.

We note that the VMI is obtained by considering the attenuation weights $w = \frac{M(E)}{\|M(E)\|_2}$ where the VMI energy E is chosen to maximize a given metric, for example, the CNR of a region of interest (ROI) in a given imaging task.

We define the CNR of a signal as the difference between the mean CT numbers of the signal and the background divided by the mean standard deviation of the signal:

$$\mathrm{CNR}(w, tp, \tau) = \frac{mean(CT\#_{signal}) - mean(CT\#_{background})}{s(w, tp, \tau)_{signal}}. \tag{17}$$

In our numerical simulations, we consider iodine inserts as our ROIs for the signal, and all parts of the image containing only water were considered as the background.

A fundamental component of our study involves calculating the mean pixel variance $s^2(w, tp, \tau)$ of the monochromatic image, and to streamline the process, we derive an analytical expression for it in the following. Let L denote the total number of lines (bins $\times$ views). If the monochromatic sinograms (16) corresponding to different lines are considered independent, then their covariance, which is denoted by Σ_{mono} and is of size $L \times L$, is a diagonal matrix of monochromatic variances

$$\sigma_l^2(w, tp, \tau) = w^t\Sigma_l w. \tag{18}$$

The pixel covariance matrix is then given by

$$\Sigma_y = B\Sigma_{mono}B^t, \tag{19}$$

where $B = (b_{pl})_{1\le p\le P,\ 1\le l\le L}$ is the FBP matrix.

By direct calculation, we obtain that

$$(\Sigma_y)_{ii} = \sum_{l=1}^{L}\sigma_l^2(w, tp, \tau)b_{pl}^2, \quad i = 1, \dots, P. \tag{20}$$

Therefore, the mean pixel variance of the monochromatic signal is given by

$$\begin{aligned} s^2(w, tp, \tau) &= \frac{1}{P}\sum_{p=1}^{P}(\Sigma_y)_{ii} = \frac{1}{P}\sum_{p=1}^{P}\sum_{l=1}^{L}\sigma_l^2(w, tp, \tau)b_{pl}^2 \\ &= \frac{1}{P}\sum_{l=1}^{L}\left(\sum_{p=1}^{P}b_{pl}^2\right)\sigma_l^2(w, tp, \tau) \\ &= \frac{1}{P}\sum_{l=1}^{L}(b_l^tb_l)\sigma_l^2(w, tp, \tau), \end{aligned} \tag{21}$$

where b_l denote the l-th column of B. Now using Equation (18), we obtain that

$$\begin{aligned} s^2(w, tp, \tau) &= \frac{1}{P}\sum_{l=1}^{L}(b_l^tb_l)w^t\Sigma_l w \\ &= w^t\left(\frac{1}{P}\sum_{l=1}^{L}b_l^tb_l\Sigma_l\right)w = w^tQw, \end{aligned} \tag{22}$$

since

$$q_{ij} = \frac{1}{P}\mathrm{tr}(\mathrm{BC}^{(ij)}\mathrm{B}^{t}) = \frac{1}{P}\sum_{l=1}^{L}\sum_{p=1}^{P} b_{pl}^{2}(\Sigma_l)_{ij}$$

$$= \frac{1}{P}\sum_{l=1}^{L} b_l^t b_l(\Sigma_l)_{ij}, \quad j = 1, 2. \tag{23}$$

2.5 | Minimization of mean pixel variance

In the following, we show that the smallest eigenvalue of the mean pixel covariance matrix Q gives the minimum mean variance in the monochromatic image. Thus, it can be used as an objective function in determining the optimal tube settings for noise minimization, which simplifies the optimization task.

We first observe that if $\det J(x_l) \neq 0$ for all l, then Σ_l is positive definite for all l, and thus the matrix $Q = \frac{1}{P}\sum_{l=1}^{L} b_l^t b_l \Sigma_l$ is positive definite. This implies that $s^2(w, tp, \tau) = w^t Q w$ is a positive definite quadratic form. This implies by the spectral theorem that it is orthogonally diagonalizable, that is the eigenvectors of Q form an orthogonal basis for $\mathbb{R}^2$ (see e.g., Horn and Johnson[27]).

For $i = 1, 2$, we let $Qu_i = \lambda_i u_i$ where $\|u_i\|_2 = 1$, and $\lambda_1 \geq \lambda_2 > 0$, that is, u_i is the unit eigenvector associated to eigenvalue λ_i. Then, for each tube potential pair tp and fluence τ,

$$\min_{\|w\|_2=1} s^2(w, tp, \tau) = \min_{\|w\|_2=1} w^t Q(tp, \tau) w = \lambda_2(tp, \tau), \tag{24}$$

where the minimizer is $u_2(tp, \tau)$. One can then minimize λ_2 over tp and τ to find the optimal tube potential pair and the photon fluence. Hence,

$$(w^*, tp^*, \tau^*) = \arg\min_{w,tp,\tau} s^2(w, tp, \tau), \tag{25}$$

where

$$(tp^*, \tau^*) = \arg\min_{tp,\tau} \lambda_2(tp, \tau), \tag{26}$$

and w^* is the unit eigenvector of $Q(tp^*, \tau^*)$ corresponding to $\lambda_2(tp^*, \tau^*)$.

We observe that scan parameters that maximize Jacobian determinant values over the set of expected line integrals minimize the mean pixel variance. Indeed, equations (12) and (23) imply that the entries of the matrix Q are inversely proportional to the square of the Jacobian determinant values. Thus, if the Jacobian determinant values increase, then the diagonal entries of (Σ_l and hence) Q decrease. Since the smallest diagonal entry provides an upper bound for the smallest eigenvalue (see e.g., Horn and Johnson[27]), we conclude that scan parameters that maximize Jacobian determinant values minimize the small eigenvalue of Q and hence it reduces the mean pixel variance.

Finally, we would like to add a remark regarding the minimization of the mean pixel variance (24). In forming the VMI, the material basis weights are restricted to the corresponding physical attenuation values. In general, we could remove this constraint and perform minimization of pixel variance in a VMI-like image where any weighted combination of material basis images is considered. Doing so should allow further reduction in the final image pixel variance. However, for the iodine-water material pair, we numerically observed that this is not the case. More specifically, there is E^* such that $\frac{M(E^*)}{\|M(E^*)\|_2} = w^*$. This is mainly because $M_1(E) > M_2(E)$ for all E in the diagnostic energy range, the ratio $M_1(E)/M_2(E)$ varies substantially in this energy range, and the components of w^* have the same sign. We thus have

$$\min_{0<E<E_{max}} s^2(E, tp, \tau) = \min_{\|w\|_2=1} s^2(w, tp, \tau) = \lambda_2(tp, \tau). \tag{27}$$

We caution that this result is specific to iodine-water material pair and may not hold for other material basis pairs.

TABLE 1 Phantom configuration.

Material	Center (cm)	Radius (cm)
0.1% Iodine	(−1,1)	0.3
0.2% Iodine	(1,1)	0.3
0.5% Iodine	(1,−1)	0.3
1% Iodine	(−1, −1)	0.3
Calcium	(−2,0)	0.1
Calcium	(0,−2)	0.2
Calcium	(2,0)	0.3
Calcium	(0,2)	0.4
Water	(0,0)	3.6

2.6 | Simulation setup

In the numerical simulations, we used a $8 \times 8\ cm^2$ phantom consisting of a large water disk with inserted iodine-solution and calcium disk signals (see Figure 4). The centers and radii of each disk, and the concentration of iodine solutions are given in Table 1 For the phantom shown in Figure 4, the DECT measurements were numerically simulated for 512×512 lines (bins $\times$ views) in fan beam geometry. The distance from source to detector was 100 cm. For each line, 100 realizations

were obtained by considering a compound Poisson process.[19] The voltage range of x-ray tubes was considered to be 30–150 kV, with energy bin widths of 1 keV. The material for the x-ray beam filter was set at 2 mm of aluminum. The results were not significantly affected by variations in the total number of photons and fluence between low and high kV scans. As a result, these factors were considered equal in the analysis, that is, $\tau = T/2$.

In our numerical simulations, we analytically calculated the CNR separately for all iodine inserts in the VMI based on optimal energy, employing Equation (17). We defined the iodine disks as our ROIs for the signal, while the background ROI encompassed all areas in the VMI image containing only water (see Figure 4 and Table 1). To assess the accuracy of the analytical approach, we additionally computed 0.1% Iodine CNR using images reconstructed from DECT measurements across 100 noise realizations.

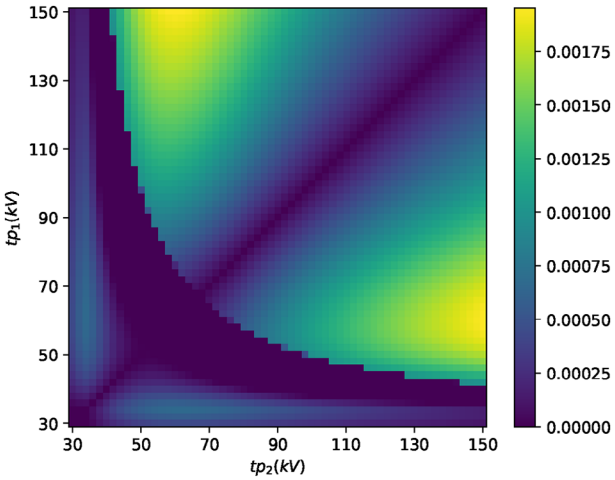

FIGURE 1 The minimum of absolute value of Jacobian determinants over line integral values up to 0.01 and 7.2 g/cm^2, for iodine and water respectively, as a function of tube settings varying from 30 to 150 kV.

3 | RESULTS

In this section, we present the results of our numerical experiments conducted for the iodine-water material pair. We then demonstrate the dependence of uniqueness to the Jacobian determinant values and showcase a non-unique sinogram estimation. We finally provide our numerical results on the optimization of the x-ray tube settings and VMI energy to maximize iodine CNR.

3.1 | Uniqueness of the reconstructed sinograms

As mentioned in Section 2.2, the uniqueness of line-integral estimation is ensured if the Jacobian determinant is nonzero everywhere in the rectangle containing all expected noiseless line integral values. Jacobian determinant values vary according to the chosen tube potentials and the filters of the x-ray energy spectra, where we fix the latter and focus on examining the effect of the former.

According to the Equations (12) and (15), the sinogram (co-)variances are inversely proportional to the square of the Jacobian determinant. In Figure 1, we present the plot of the quantity

$$\min_{x\in\mathcal{R}} |\det J(x)|. \tag{28}$$

This is the minimum of absolute values of Jacobian determinant over the rectangular region $\mathcal{R} = [0, 0.01] \times [0, 7.2]$ (g/cm^2), which corresponds to the range of line integral values for iodine and water obtained from our phantom (depicted in Figure 4). We caution that the Jacobian determinant also depends on the tube settings, although we omit the specific notation for simplicity.

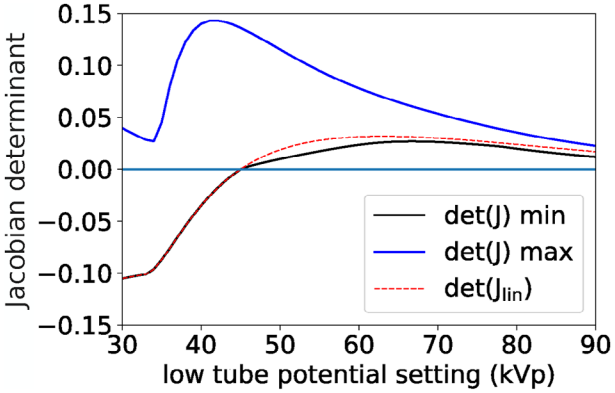

FIGURE 2 Plot of the Jacobian determinant for the sinogram-to-DECT mapping. The black and blue curves show the minimal and maximal values of Jacobian determinant over the line integral values of the phantoms shown in 1, respectively. The red curve corresponds to the Jacobian determinant values for $x = 0$. For the shown results, the high tube potential is 120 kV, and the low tube potential ranges from 30 to 90 kV, simulated in 1 keV increments. DECT, Dual-energy CT.

Figure 1 reveals that light green/yellow regions, which correspond to higher absolute values of the Jacobian determinant, indicate tube potentials that lead to more stable inversion of the sinogram-to-DECT mapping. Therefore, the use of the tube potentials in the region $50 \le tp_1 \le 80$ (kV) and $120 \le tp_2 \le 150$ (kV) yield more stable sinogram estimation.

In Figure 2, for low tube setting varying from 30 to 90 kV and a high tube setting of $tp_2 = 120$ kV, we plot in black and blue the minimal and maximal Jacobian determinant values attained over the set of all values of line integrals of the phantoms shown in Figure 4. The red

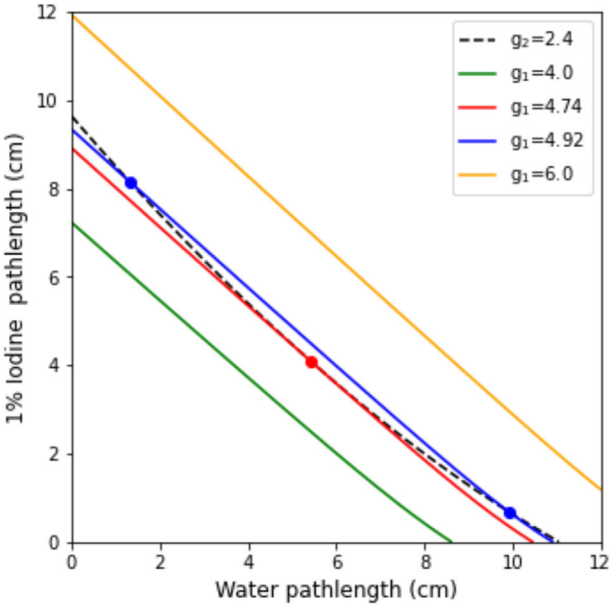

FIGURE 3 Plot of the level curves of the log-intensity measurements as a function of the water and iodine line integral values demonstrating the existence of singular solutions to the inverse sinograms-to-DECT measurements map. The red dot is a point where the Jacobian vanishes. The dashed black curve ($g_2 = 2.4$ g/cm^2) intersects the blue one ($g_1 = 4.92$ g/cm^2) at two twice (shown with blue dots), so both line integral value pairs lead to the same log-intensity measurement value of $(g_1, g_2) = (4.92, 2.4)$ (g/cm^2). DECT, Dual-energy CT.

curve represents the Jacobian determinant values for $x = 0$, which also corresponds to Jacobian determinant of the linearization (i.e., the first order Taylor expansion) of the map $g(x)$ (4) around $x = 0$.

We observe in Figure 2 that if the low tube potential is less than 45 kV, the Jacobian determinant vanishes somewhere inside the rectangle, and hence the uniqueness of sinogram estimation is not guaranteed. In fact, for the tube potential pair $(tp_1, tp_2) = (35, 120)$ (kV), for which the Jacobian determinant becomes zero near the line integral values $x = (x_1, x_2) = (4, 6)$ (g/cm^2), we encountered singular solutions to the inverse sinograms-to-DECT measurements map. In Figure 3, we show some of the level curves of the corresponding log-intensity measurements as a function of the iodine and water line integral values. The red dot is where the Jacobian determinant is zero. The level curve for $g_2 = 2.4$ g/cm^2 (shown in dashed black) intersects the level curve for $g_1 = 4.92$ g/cm^2 (shown in blue) at two points (shown with blue dots). This means that two different line integral value pairs (shown with blue dots) lead to the same measurement value of $(g_1, g_2) = (4.92, 2.4)$ (g/cm^2).

The presence of non-uniqueness in the sinogram-to-DECT mapping has implications for the design of its inversion algorithm; namely, other information such as sinogram values at neighboring pixels needs to be taken into account in order for the correct solution to be identified. Furthermore, the algorithm robustness testing needs to account for the impact of data inconsistency from physical factors such as noise on its ability to identify the correct solution.

3.2 | Optimization of the iodine CNR in virtual monochromatic images

In this section, we present the results of the analysis conducted on the CNR values of each iodine disk in the VMI. In each case, we used the iodine disk as the signal ROI. For the background ROI, we considered all parts of the image that contains only water (see Figure 4

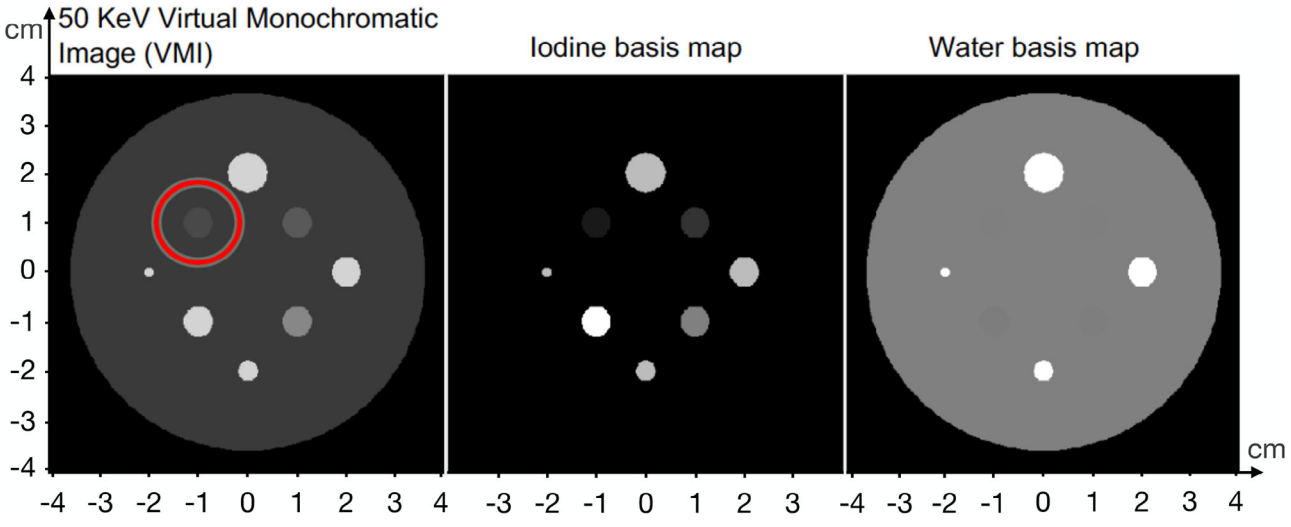

FIGURE 4 The plot of the circular water phantom with inserted iodine-solutions and calcium rods. The red circle indicates the disk with the lowest iodine concentration (0.1%), where CNR analysis is more critical. CNR, contrast-to-noise ratio.

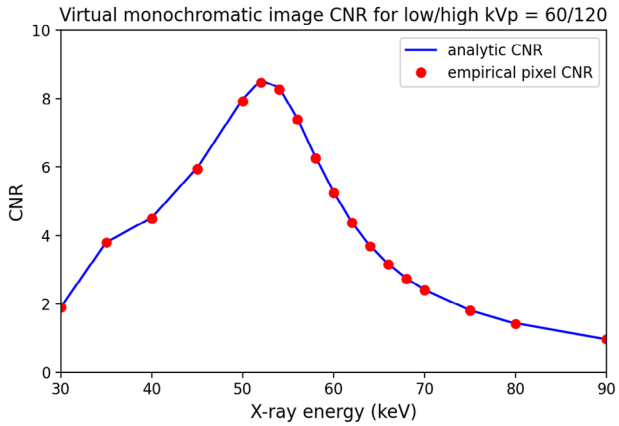

FIGURE 5 For low/high tube settings of 60/120 kV, the CNR of the 0.1% Iodine disk is shown for a noise level of 50 000 photons incident on each detector pixel. The blue curve represents CNR values computed analytically, while the red dots correspond to CNR values obtained via image reconstruction for 100 noise realizations. CNR, contrast-to-noise ratio.

and Table 1). The CNR values were computed using Equation (17) analytically and also by using the reconstructed images from 100 noise realizations in order to test the accuracy of the analytic approach. Figure 5 displays these CNR values for the low and high tube settings of 60/120 kV, with the blue curve representing the analytically computed values and the red dots indicating the CNR values obtained from the reconstructed images. Notably, there is a remarkable agreement between the two approaches. Furthermore, the maximum CNR for the 0.1% Iodine disk in the VMI was observed at an energy level of 53 keV. Similar results were obtained for the 60/140 kV setting. These findings provide valuable insights into the optimal energy range for maximizing CNR in VMI.

To further demonstrate the influence of tube potentials on the CNR, we present in Figure 6 the optimal CNR values of all iodine disks for various tube settings. Comparing the high tube potential settings of 120 kV and 140 kV, it is observed that the former yields slightly higher CNR values for each of the iodine disks. Hence, within the scope of this study, the tube potential pair of 60/120 kV emerges as the optimal choice for maximizing the iodine CNR in VMI, regardless of the iodine concentration amount.

We remark that, in view of Figure 1, this pair of tube potentials lead to stable inversion of the sinogram-to-DECT mapping. This result highlights the significance of selecting the appropriate kV settings to optimize the visualization and diagnostic quality of iodine in VMI imaging. We finally note that the maximum CNR value for each of the iodine disks in the VMI was obtained at an energy level of 53–54 keV.

4 | DISCUSSION AND CONCLUSIONS

DECT systems have upgraded standard CT by simultaneously capturing two spectral measurements, enabling enhanced material-specific information and contrast agent usage.[1–5]

In this study, we showed that the selection of DECT scan parameters, including x-ray tube settings and fluence, significantly impacts CNR and overall image quality. To this end, we developed a systematic approach to determine optimal x-ray tube settings for DECT scans while keeping subject size and total radiation dose constant. Our goal was to minimize noise and maximize CNR in material density images, with a specific focus on iodine-based CNR.

Our analytical framework involved examining noise propagation from DECT measurements to material density images. We analyzed a noise model based on a compound Poisson process for DECT measurements and linearized the inverse sinogram-to-DECT mapping. This allowed us to derive analytic expressions for sinogram and mean image variances, as well as CNR, as functions of tube potentials, fluence, and VMI energy.

Our DECT simulations were based on dual source DECT scanners. However, our theoretical framework is applicable to dual-layer detectors and photon counting detectors as well. In those cases, one needs to optimize the energy window thresholds instead of the tube potentials. The photon fluence was taken into account in our theoretical framework. However, we considered equal times for both energy measurement in the numerical simulations as its influence on the results was not significant.

One of our key goals was the identification of optimal x-ray tube settings that maximize the square of Jacobian determinant values over a domain of interest, resulting in improved stability of basis material reconstructions. Additionally, we determined ideal x-ray tube settings and the VMI energy for maximal CNR, which was found to be the least noisy VMI synthesized from iodine and water density images. Importantly, these findings suggest that using more general weights to linearly combine these images does not substantially enhance image quality.

We also highlighted instances of non-uniqueness in DECT, focusing on situations where the Jacobian determinant becomes zero within the domain of interest despite significant separation in x-ray spectra. This phenomenon leads to singular solutions when attempting to invert the sinograms-to-DECT measurements mapping. Our observation aligns with previous work by Alvarez,[9] who analyzed the invertibility of the sinogram-to-DECT mapping, and Levine,[8] who first provided examples of non-unique solutions in DECT. Our findings further underscore the significance of carefully considering the uniqueness properties of DECT line-integral estimation when selecting scan parameters.

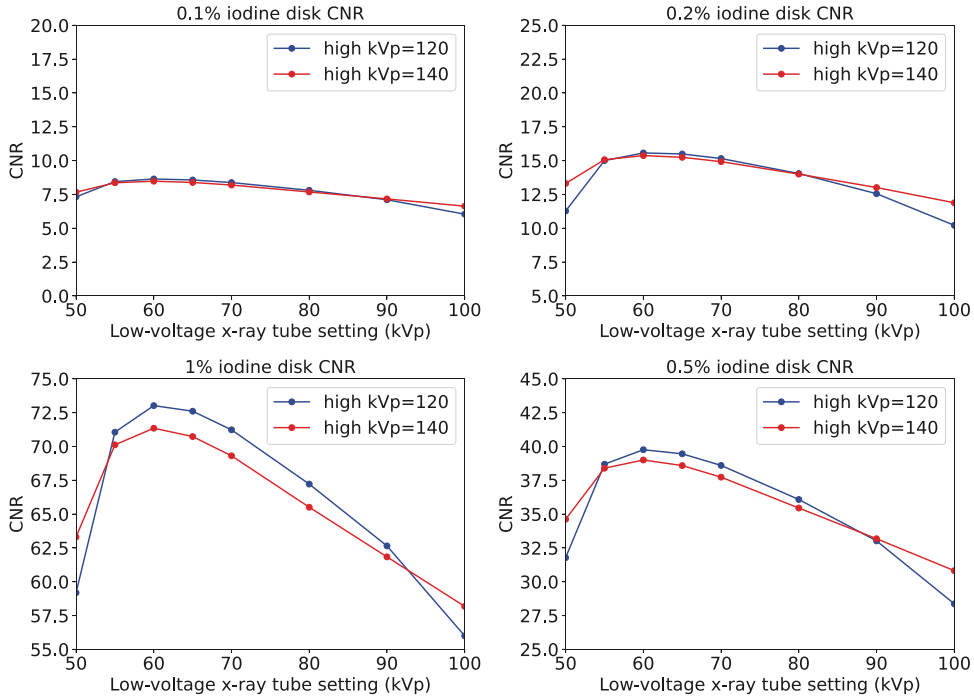

FIGURE 6 The maximal CNR values for each iodine disk in VMI, optimized over VMI energy for given tube potential pairs. Shown in the plot are only the high tube voltages of 120 and 140 kV; the low tube voltage is indicated on the x-axis. Of the values computed, the 60/120 kV setting allows for maximum iodine CNR for all inserts. CNR, contrast-to-noise ratio; VMI, virtual monochromatic images.

Our approach distinguishes itself from previous studies which primarily used empirical optimization or denoising techniques.[12–16] Alternatively, we employed an analytical methodology to analyze noise propagation, derive variance expressions, and utilize them to optimize tube settings. This allowed us to identify optimal tube potentials and VMI energy for maximal CNR and the least noisy monochromatic images.

Our primary objective in this research was to propose a framework for optimizing DECT scan parameters to achieve maximum stability of reconstructions and CNR. While our theoretical framework is applicable to any DECT imaging task, our numerical outcomes are specific to the phantom used as it determines the upper bound for the expected line integral values and consequently the range of Jacobian values observed. Therefore, it is important to consider the specific imaging task at hand and carefully assess all relevant factors when implementing this framework.

In conclusion, our study presents a comprehensive framework for optimizing DECT scan parameters to maximize iodine-based CNR and improving image quality for a given object size and radiation dose. By considering noise propagation and analytical derivations, we have identified optimal tube settings and VMI energy, shedding light on the importance of tailored parameter selection in DECT imaging. Our work contributes to the broader understanding of DECT parameter optimization, facilitating its practical implementation in clinical settings.

In future studies, we plan to validate our theoretical results using real DECT data and extend our analysis to cases involving three or more materials and energy measurements.

ACKNOWLEDGMENTS

This work was supported in part by NSF DMS grants 2206279, 2306411 and 1908736, and NIH Grant Nos. R01-EB023968 and R21-CA263660. The contents of this article are solely the responsibility of the authors and do not necessarily represent the official views of the National Institutes of Health.

CONFLICT OF INTEREST STATEMENT

The authors have no conflicts to disclose.

REFERENCES

1. Grant KL, Flohr TG, Krauss B, Sedlmair M, Thomas C, Schmidt B. Assessment of an advanced image-based technique to calculate virtual monoenergetic computed tomographic images from a dual-energy examination to improve contrast-to-noise ratio in examinations using iodinated contrast media. *Invest Radiol*. 2014;49:586-592.
2. Leng S, Yu L, Fletcher JG, McCollough CH. Maximizing iodine contrast-to-noise ratios in abdominal CT imaging through use of energy domain noise reduction and virtual monoenergetic dual-energy CT. *Radiology*. 2015;276:562.
3. Kalisz K, Rassouli N, Dhanantwari A, Jordan D, Rajiah P. Noise characteristics of virtual monoenergetic images from a novel detector-based spectral CT scanner. *Eur J Radiol*. 2018;98:118-125.

4. Sakabe D, Funama Y, Taguchi K, et al. Image quality characteristics for virtual monoenergetic images using dual-layer spectral detector CT: comparison with conventional tube-voltage images. *Physica Med*. 2018;49:5-10.
5. Tabari A, Gee MS, Singh R, et al. Reducing radiation dose and contrast medium volume with application of dual-energy CT in children and young adults. *Am J Roentgenol*. 2020;214:1199-1205.
6. Hounsfield GN. Computerized transverse axial scanning (tomography): Part 1. Description of system. *Br J Radiol*. 1973;46:1016-1022.
7. Alvarez RE, Macovski A. Energy-selective reconstructions in x-ray computerised tomography. *Phys Med Biol*. 1976;21:733.
8. Levine ZH. Nonuniqueness in dual-energy CT. *Med Phys*. 2017;44:e202-e206.
9. Alvarez RE. Invertibility of the dual energy x-ray data transform. *Med Phys*. 2019;46:93-103.
10. Bal G, Terzioglu F. Uniqueness criteria in multi-energy CT. *Inverse Problems*. 2020;36:065006.
11. Bal G, Gong R, Terzioglu F. An inversion algorithm for P-functions with applications to multi-energy CT. *Inverse Problems*. 2022;38:035011.
12. Tao S, Rajendran K, Zhou W, Fletcher JG, McCollough CH, Leng S. Improving iodine contrast to noise ratio using virtual monoenergetic imaging and prior-knowledge-aware iterative denoising (mono-PKAID). *Phys Med Biol*. 2019;64:105014.
13. Yu L, Primak AN, Liu X, McCollough CH. Image quality optimization and evaluation of linearly mixed images in dual-source, dual-energy CT. *Med Phys*. 2009;36:1019-1024.
14. Yu L, Christner JA, Leng S, Wang J, Fletcher JG, McCollough CH. Virtual monochromatic imaging in dual-source dual-energy CT: radiation dose and image quality. *Med Phys*. 2011;38:6371-6379.
15. Michalak G, Grimes J, Fletcher J, et al. Selection of optimal tube potential settings for dual-energy CT virtual mono-energetic imaging of iodine in the abdomen. *Abdom Radiol*. 2017;42:2289-2296.
16. Dabli D, Frandon J, Hamard A, et al. Optimization of image quality and accuracy of low iodine concentration quantification as function of kVp pairs for abdominal imaging using dual-source CT: a phantom study. *Physica Med*. 2021;88:285-292.
17. Ren Y, Xie H, Long W, Yang X, Tang X. On the Conditioning of spectral channelization (Energy Binning) and its impact on multi-material decomposition based spectral imaging in photon-counting CT. *IEEE Trans Biomed Eng*. 2021;68:2678-2688.
18. Williamson JF, Li S, Devic S, Whiting BR, Lerma FA. On two-parameter models of photon cross sections: application to dual-energy CT imaging. *Med Phys*. 2006;33:4115-4129.
19. Whiting BR. Signal statistics in x-ray computed tomography. In: *Medical Imaging 2002: Physics of Medical Imaging*. Vol 4682. International Society for Optics and Photonics; 2002:53-60.
20. Hubbell JH, Seltzer SM. *Tables of X-ray mass attenuation coefficients and mass energy-absorption coefficients 1 keV to 20 MeV for elements Z= 1 to 92 and 48 additional substances of dosimetric interest*. Technical report, National Inst. of Standards and Technology-PL; 1995.
21. Poludniowski G, Omar A, Bujila R, Andreo P. SpekPy v2. 0–a software toolkit for modeling x-ray tube spectra. *Med Phys*. 2021;48:3630-3637.
22. Gale D, Nikaido H. The Jacobian matrix and global univalence of mappings. *Math Ann*. 1965;159:81-93.
23. Garcia C, Zangwill W. *On univalence and P-matrices*. Vol. Report 7737, Center for Mathematical Studies in Business and Economics; 1977.
24. Mas-Colell A. Homeomorphisms of compact, convex sets and the Jacobian matrix. *SIAM J Math Anal*. 1979;10:1105-1109.
25. Cowan G. *Statistical Data Analysis*. Oxford University Press; 1998.
26. Roessl E, Ziegler A, Proksa R. On the influence of noise correlations in measurement data on basis image noise in dual-energylike x-ray imaging. *Med Phys*. 2007;34:959-966.
27. Horn RA, Johnson CR. *Matrix Analysis*. Cambridge University Press; 2012.

How to cite this article: Terzioglu F, Sidky EY, Phillips JP, Reiser IS, Bal G, Pan X. Optimizing dual-energy CT technique for iodine-based contrast-to-noise ratio, a theoretical study. *Med Phys*. 2024;51:2871–2881.
https://doi.org/10.1002/mp.17010